Journal of Controlled Release 224 (2016) 77–85

Contents lists available at ScienceDirect

Journal of Controlled Release

journal homepage: www.elsevier.com/locate/jconrel

PEGylated and targeted extracellular vesicles display enhanced cell specificity and circulation time

S.A.A. Kooijmans [a], L.A.L. Fliervoet [b], R. van der Meel [a,c], M.H.A.M. Fens [a], H.F.G. Heijnen [a], P.M.P. van Bergen en Henegouwen [d], P. Vader [a], R.M. Schiffelers [a,*]

[a] Department of Clinical Chemistry and Haematology, University Medical Center Utrecht, Utrecht, The Netherlands
[b] Department of Pharmaceutics, Utrecht Institute for Pharmaceutical Sciences, University of Utrecht, Utrecht, The Netherlands
[c] Department of Biochemistry and Molecular Biology, The University of British Columbia, Vancouver, British Columbia V6T 1Z3, Canada
[d] Division of Cell Biology, Department of Biology, Utrecht University, Utrecht, The Netherlands

ARTICLE INFO

Article history:
Received 27 November 2015
Received in revised form 4 January 2016
Accepted 5 January 2016
Available online 7 January 2016

Keywords:
Extracellular vesicles
Drug delivery
Polyethylene glycol
Circulation time
Targeting
Nanobody

ABSTRACT

Extracellular vesicles (EVs) are increasingly being recognized as candidate drug delivery systems due to their ability to functionally transfer biological cargo between cells. However, the therapeutic applicability of EVs may be limited due to a lack of cell-targeting specificity and rapid clearance of exogenous EVs from the circulation. In order to improve EV characteristics for drug delivery to tumor cells, we have developed a novel method for decorating EVs with targeting ligands conjugated to polyethylene glycol (PEG). Nanobodies specific for the epidermal growth factor receptor (EGFR) were conjugated to phospholipid (DMPE)-PEG derivatives to prepare nanobody-PEG-micelles. When micelles were mixed with EVs derived from Neuro2A cells or platelets, a temperature-dependent transfer of nanobody-PEG-lipids to the EV membranes was observed, indicative of a 'post-insertion' mechanism. This process did not affect EV morphology, size distribution, or protein composition. After introduction of PEG-conjugated control nanobodies to EVs, cellular binding was compromised due to the shielding properties of PEG. However, specific binding to EGFR-overexpressing tumor cells was dramatically increased when EGFR-specific nanobodies were employed. Moreover, whereas unmodified EVs were rapidly cleared from the circulation within 10 min after intravenous injection in mice, EVs modified with nanobody-PEG-lipids were still detectable in plasma for longer than 60 min post-injection. In conclusion, we propose post-insertion as a novel technique to confer targeting capacity to isolated EVs, circumventing the requirement to modify EV-secreting cells. Importantly, insertion of ligand-conjugated PEG-derivatized phospholipids in EV membranes equips EVs with improved cell specificity and prolonged circulation times, potentially increasing EV accumulation in targeted tissues and improving cargo delivery.

1. Introduction

Over the past decade extracellular vesicles (EVs) have increasingly gained attention as candidate drug delivery systems due to their unique properties. As extensively reviewed elsewhere [1–4], EVs are lipid bilayer-surrounded vesicles released by many, if not all, cell types in the body. They are heterogeneous in terms of protein, nucleic acid and lipid composition, with sizes ranging from 30 to 1000 nm. EVs can be subdivided in different classes based on intracellular origin, e.g. microvesicles (or ectosomes) are released through direct budding of the plasma membrane, while exosomes are released from endosomal compartments upon fusion with the plasma membrane [5,6]. EVs have been implicated in intercellular communication, and are believed to be capable of functionally transferring condensed packages of biological cargo (e.g. miRNA, mRNA and proteins) to target cells and tissues [1,7]. These characteristics make EVs ideal candidate delivery systems for therapeutic nucleic acids (e.g. siRNA and miRNA). Hence, it is not surprising that therapeutic applications of EVs are a topic of intense investigation, and the first clinical trials with EVs are emerging [8].

Although EVs harbor potential advantages for drug delivery over conventional drug delivery systems, such as biological tolerability and the ability to induce phenotypical changes in recipient cells [1,9], major challenges for their therapeutic applicability remain. Due to their highly complex and variable composition, cell specificity and biological effects of EVs can be unpredictable [10]. These could manifest as off-target effects when EVs are employed as drug carriers. To limit such effects and promote therapeutic efficacy, EVs may be equipped with

* Corresponding author at: Department of Clinical Chemistry and Haematology, Correspondence G03.550, University Medical Center Utrecht, Heidelberglaan 100, 3508 GA Utrecht, The Netherlands.
E-mail address: r.schiffelers@umcutrecht.nl (R.M. Schiffelers).

http://dx.doi.org/10.1016/j.jconrel.2016.01.009
0168-3659/

targeting ligands and appropriate cargos. Such modifications have been explored in several studies, which showed successful targeted drug delivery using EVs and underlined their therapeutic potential [11–16].

A popular strategy to decorate EVs with targeting ligands is the transfection of EV-producing cells to drive expression of targeting moieties fused with EV membrane proteins, such as Lamp2b [11,17,18]. Although effective, such strategies are hampered by the requirement to modify producer cells, which often is time-consuming and challenging, especially when using primary cells. In addition, some targeting ligands are prone to improper expression and degradation, which limits their functional display on EVs [17]. Moreover, while decoration of EVs with targeting ligands usually improves target cell interactions, it does not necessarily prevent interactions with other, non-target cells, allowing nonspecific uptake and related off-target effects. To overcome such issues, we here propose a novel method to provide stealth as well as tumor cell-targeting characteristics to pre-isolated EVs, based on the 'post-insertion' method previously applied to functionalize liposomes [19]. The hydrophilic polymer polyethylene glycol (PEG) is well known to shield nanoparticles from interactions with plasma proteins and improve circulation time [20,21]. We hypothesized that these features would be beneficial for EV-based drug delivery systems, given that exogenously administered EVs have been described to be rapidly cleared from the circulation by the reticulo-endothelial system (RES) [22], limiting their accumulation in target tissue. Furthermore, we employed nanobodies against the epidermal growth factor receptor (EGFR) as model targeting ligands. This receptor is overexpressed in a range of solid tumors and is an established target for cancer therapy with several inhibitors used in the clinic [23,24]. Nanobodies are single variable domains derived from the heavy chains (VH) of *Camelidae* heavy (H) chain antibodies, and are therefore also termed VHHs or single-domain antibodies (sdAbs) [25]. These 15 kD fragments possess the full antigen-binding capacity of the original antibody, and have other favorable characteristics compared with conventional antibodies, such as high solubility and resistance to extreme thermal and chemical conditions [26,27]. Here, we evaluated how introduction of polyethylene glycol (PEG)-conjugated nanobodies onto EVs via post-insertion affects EV characteristics, in vitro interactions with tumor cells, and in vivo circulation time and tissue distribution in tumor-bearing mice.

2. Materials and methods

2.1. Materials

1,2-Distearoyl-sn-glycero-3-phosphoethanolamine (DSPE)-PEG, MW 2000 and 1,2-Dimyristoyl-sn-glycero-3-phosphoethanolamine (DMPE)-PEG-maleimide, MW 3400 were purchased from Nanocs Inc. (New York, USA). 1,1″-dioctadecyl-3,3, 3″,3″-tetramethylindotricarbocyanine iodide (DiR), MicroBCA Protein Assay Kit, *N*-succinimidyl S-acetylthioacetate (SATA) and CellTracker Deep Red dye were obtained from Thermo Fisher Scientific (Waltham, USA). Sepharose CL-4B was ordered from Sigma-Aldrich (Steinheim, Germany). pET28a vectors encoding EGa1 and R2 Myc-tagged nanobodies were kindly provided by Dr. S. Oliveira (Department of Biology, Utrecht University, Utrecht, The Netherlands).

2.2. Nanobody production

R2 and EGa1 nanobodies were expressed and purified as described previously [28], with minor modifications. pET28a expression vectors, containing a pelB leader sequence followed by a nanobody sequence with C-terminal c-Myc- and His_6-tags for detection and purification, respectively, were introduced in BL21 Star (DE3)pLysS chemically competent *E. coli* (Thermo Fisher Scientific). Cells were grown overnight in shaking cultures at 37 °C in 2xYT medium supplemented with 2% (w/v) glucose and selection antibiotics. A 5L Bioflo 115 fermentor (Eppendorf, Germany) with ZYP-5052 auto induction medium (described in [29]) was inoculated with the overnight culture and cells were grown for several hours at 37 °C until log phase was observed. The culture was incubated for 22 h at 22 °C, and protein was extracted from the periplasmic space with lysis buffer (25 mM HEPES, 0.5 M NaCl, 1 μg/mL DNase I, 10 mM $MgCl_2$, pH 7.8) in three freeze–thaw cycles using liquid nitrogen. After removal of insoluble material by centrifugation at 10,000 ×*g* and 4 °C for 1 h, nanobodies were extracted overnight at 4 °C with TALON Superflow IMAC resin (Clontech Laboratories, Inc). Nanobodies were eluted from the resin with elution buffer (25 mM HEPES, 0.5 M NaCl, 500 mM imidazole) and further purified in HEPES-buffered saline (HBS) on an ÄKTA FPLC system (GE Healthcare Europe GmbH, Germany) coupled to a HiLoad 26/60 Superdex gel filtration column (GE Healthcare). Protein concentrations were measured by spectrophotometry at 280 nm, using molar extinction coefficients calculated via the online ProtParam tool (web.expasy.org/protparam/). Purity of the nanobodies was verified by PageBlue staining after SDS-PAGE.

2.3. Preparation of nanobody-PEG micelles

Reactive sulfhydryl groups were introduced to the nanobodies with SATA as described elsewhere [30]. Unconjugated SATA was removed using Zeba Spin desalting columns with a 7 kD MWCO (Thermo Fisher Scientific). DMPE-PEG-maleimide and DSPE-PEG were dissolved in a 1:1 molar ratio in HEPES buffer (10 mM HEPES, 135 mM NaCl, pH 7.4) for 15 min at 60 °C to form micelles. After deprotection of the sulfhydryl groups, nanobodies were conjugated to the micelles in a 8.6:1000 molar ratio of nanobody:DMPE-PEG-maleimide overnight at 4 °C. Unreacted maleimide groups were quenched by addition of a 20-fold molar excess of β-mercaptoethanol, and free nanobodies were removed by four washing steps on 100 kD MWCO Vivaspin tubes (Sartorius, UK). Traces of β-mercaptoethanol were removed by overnight dialysis against excess HBS in 10 kD Slide-A-Lyzer cassettes (Thermo Scientific). Micelles were redissolved at 60 °C for 10 min, followed by sonication with 10 μm amplitude for 2 × 5 s in a Soniprep 150 sonicator (MSE, UK) to reduce micelle size and facilitate upstream separation from EVs. Concentration of nanobodies on the micelles was estimated using a MicroBCA Protein Assay according to the manufacturer's instructions. Micelles were stored at 4 °C and used within 2 weeks.

2.4. Cell culture and EV isolation

Human epidermoid carcinoma cells (A431, ATCC, Manassas, USA) were cultured at 37 °C and 5% CO_2 in Dulbecco's Modified Eagle Medium (DMEM) supplemented with 10% fetal bovine serum (FBS) and 100 U/mL penicillin and 100 U/mL streptomycin. Mouse neuroblastoma cells (Neuro2A, ATCC) were maintained under the same conditions in Roswell Park Memorial Institute (RPMI) 1640 medium supplemented with 10% FBS and antibiotics. For EV production, Neuro2A cells were seeded at an appropriate density in EV-depleted medium (which contained FBS depleted from EVs by overnight centrifugation at 100 000 ×*g* at 4 °C). Cells were allowed to produce EVs and after 72 h, when cells reached 90–95% confluency, EVs were isolated with a differential (ultra)centrifugation method as previously described [31]. The washed EV pellet after the final 100,000 ×*g* step was resuspended in phosphate-buffered saline (PBS). EV aggregates resulting from ultracentrifugation were removed by centrifugation at 1000 g for 10 min at 4 °C. EV protein concentration was determined with a MicroBCA Protein Assay.

2.5. Introduction of nanobody-PEG-lipids on EVs using post-insertion

EVs were mixed with nanobody-PEG micelles in a 1:1 ratio (μg protein:μg protein) in a total volume of 100–150 μL and incubated in a GeneAmp PCR System 9700 thermocycler with heated lid for 2 h at 40 °C (unless stated otherwise). EV-micelle mixtures were cooled to

4 °C and EVs were immediately purified from free micelles by size-exclusion chromatography.

2.6. Purification of EVs by size-exclusion chromatography

For purification of EVs from free nanobody-PEG micelles, Sepharose CL-4B (Sigma-Aldrich) was packed in a XK-26/40 column (GE Healthcare) according to manufacturer's instructions. A smaller column (XK-16/20) was employed for purification of EVs from fluorescent dyes. Column was connected to an ÄKTA pure system (GE Healthcare) which was maintained at 4 °C and equilibrated with PBS. EV suspensions were injected and eluted fractions containing EVs (identified by UV absorbance at 280 nm) were pooled and concentrated using 100 kD MWCO Vivaspin tubes (Sartorius).

2.7. Western blot analysis

EV samples were mixed with sample buffer containing dithiothreitol (DTT), heated to 95 °C for 10 min and separated on 4–12% Bis–Tris polyacrylamide gels (Thermo Scientific). Proteins were electrotransferred to Immobilon-FL polyvinylidene difluoride (PVDF) membranes (Millipore). Membranes were blocked with 50% v/v Odyssey Blocking Buffer (LI-COR Biosciences) in Tris buffered saline (TBS). All immunolabeling was performed with 50% v/v Odyssey Blocking Buffer in TBS containing 0.1% Tween 20 (TBS-T). Primary antibodies were used overnight at 4 °C and included rabbit anti-CD9 antibody (Abcam, clone EPR2949, 1:2500 dilution), rabbit anti-TSG101 (Abcam, ab30871, 1:1000 dilution), mouse anti-Alix (Abcam, clone 3A9, 1:1000 dilution), rabbit-anti-EGFR (Cell Signaling Technology, clone D38B1, 1:1000 dilution) mouse-anti-β-actin (Cell Signaling Technology, clone 8H10D10, 1:1000 dilution), and mouse-anti-Myc (9E10 from MYC 1-9E10.2 hybridoma, ATCC, 1:4000). Secondary antibodies included Alexa Fluor 680-conjugated anti-rabbit antibodies (Thermo Fisher Scientific, A-21,076, 1:7500 dilution) or IRDye 800CW anti-mouse antibodies (LI-COR Biosciences, 926-32212, 1:7500 dilution). Imaging was performed on an Odyssey Infrared Imager (LI-COR Biosciences, Leusden, The Netherlands) at 700 and 800 nm, respectively.

2.8. Immuno-electron microscopy

EVs in PBS were adsorbed to carbon-coated formvar grids, fixated in a mixture of 2% paraformaldehyde and 0.2% glutaraldehyde in 0.1 M phosphate buffer, and immunolabeled with mouse anti-Myc antibody (9E10, 1:100), followed by rabbit-anti-mouse IgG (Rockland, 610-4120, 1:250) and 10 nm Protein A gold (CMC, Utrecht, The Netherlands). Grids were counterstained with uranyl-oxalate and embedded in methyl cellulose uranyl-acetate [6]. Imaging was performed using a Tecnai T12 electron microscope (FEI, Eindhoven, The Netherlands).

2.9. Nanoparticle tracking analysis

EV size distribution and concentration were determined with nanoparticle tracking analysis (NTA) using a Nanosight LM10-HS (NanoSight, UK). Before measurements, EVs were diluted to an appropriate dilution with sterile PBS (confirmed to be particle-free). Of each sample, 5 movies of 30 s were recorded using camera level 13, while temperature was maintained at 22 °C. Data was analyzed with NTA Analytical Software suite version 2.3.

2.10. Cell binding assays

To evaluate the binding of EVs to EGFR-expressing cells, EVs were mixed with 10 μM CellTracker Deep Red dye (dissolved at 2 mM in dimethyl sulfoxide (DMSO)) and incubated for 1 h at 37 °C. EVs were purified from free dye using size-exclusion chromatography. If applicable, post-insertion was performed, followed by size-exclusion chromatography and determination of protein concentration. To determine whether differences in labeling efficiency existed among samples, fluorescence of all samples was analyzed in a black 96-well plate in a Spectramax M2 microplate reader (Molecular Devices, UK) at excitation 630 nm and emission 660 nm, and compared with corresponding protein concentrations. For binding assays, A431 and Neuro2A cells were trypsinized, resuspended in ice-cold culture medium and seeded in round-bottom 96-well plates at a density of 3×10^4 cells/well. EVs were mixed with the cells at a concentration of 8 μg/mL while cells were kept on ice to inhibit cellular uptake. After 1 h, cells were collected by centrifugation at 500 g and 4 °C for 5 min. Medium was removed and cells were resuspended in ice-cold PBS with 0.3% bovine serum albumin (PBSA). This washing procedure was repeated twice and cells were resuspended in 0.2% formaldehyde in PBS. Mean fluorescence intensity of the cells was analyzed in a FACSCanto II flow cytometer (BD Biosciences, USA) and corrected for the autofluorescence of untreated cells.

2.11. In vivo circulation time and biodistribution

All animal experiments were performed with approval from the Utrecht Animal Welfare Body of the UMC Utrecht, and animal care was according to established guidelines. Sixty female Crl:NU-Foxn1^{nu} mice (20–25 g) were obtained from Charles River International Laboratories, Inc. (Germany) with free access to water and a chlorophyll-reducing chow (2016S, Harlan Laboratories, The Netherlands) to reduce organ autofluorescence. To establish human tumor xenografts, A431 cells were trypsinized, counted and suspended in ice-cold PBS. Mice were subcutaneously injected with 100 μL containing 1×10^6 cells in the right flank. Tumor growth was monitored during approximately two weeks, using a caliper to measure tumor size. Tumor volume was calculated with the formula $V = (\pi/6)LS^2$, where L and S are the largest and smallest superficial diameters, respectively. When tumors reached a volume of 200–300 mm^3, mice were injected intravenously in the tail vein with 2.5 μg DiR-labeled EVs in 100 μL PBS. EVs were labeled by mixing EV suspension with 5 μM DiR (using a DiR stock of 1 mM in DMSO), followed by incubation for 1 h at 22 °C. EVs were purified from free DiR with size-exclusion chromatography, modified with post-insertion, and purified again. To exclude the presence of aggregates, EVs were filtered through 0.45 μm syringe filters (Millipore). EV protein concentration and number was quantified with MicroBCA Protein Assay and NTA, respectively, before administration to mice. Blood samples were collected in EDTA anti-coagulated tubes by submandibular vein punctures at 1, 10, 20 and 30 min post-injection ($n = 3$ per time point). Mice were sacrificed 60 and 240 min post-injection by cervical dislocation, and additional blood samples were collected via heart puncture. Blood samples were centrifuged for 10 min at 2000 ×g and 4 °C and platelet-poor plasma was collected and stored at −80 °C. For analysis of circulation times, 35 μL of each plasma sample was transferred to a clear 384-well plate and analyzed by an Odyssey Infrared Imager at 800 nm. Quantification of fluorescent signals was performed using Odyssey software (LI-COR Biosciences). EV plasma concentrations were calculated using a standard curve of corresponding EVs spiked in normal mouse plasma. To evaluate EV biodistribution, mouse organs were collected 60 and 240 min post-injection and imaged using a Pearl Impulse Imager (LI-COR Biosciences) at the 800 nm channel. Images were analyzed by Pearl Cam software.

2.12. Statistical data analysis

When applicable, statistical data analysis was performed using IBM SPSS Statistics, version 21. Multiple-group comparisons were performed using one-way ANOVA with Tukey post-hoc tests.

3. Results

3.1. Introduction of nanobody-PEG-lipids onto extracellular vesicles via post-insertion

The nanobody EGa1 has previously been described as a high-affinity ligand for EGFR, without activating the receptor [32]. R2 is a nanobody raised against the azo-dye Reactive Red (RR6), which has been used as a non-targeting control nanobody in previous reports [28,33]. In this work, we investigated whether these nanobodies could be conjugated to PEG-phospholipid micelles, and subsequently introduced onto EVs using a post-insertion procedure (Fig. 1).

Nanobodies were first chemically modified with SATA reagent using a previously described method, to introduce sulfhydryl groups [30]. With this method, up to 8 SATA molecules (4–5 molecules on average) have been shown to be conjugated to a single nanobody molecule, without loss of affinity for the antigen [28]. The sulfhydryl groups allow nanobody conjugation to PEG-phospholipids (i.e. DMPE-PEG), which are functionalized with maleimide groups at the distal end of the PEG chains. Prior to conjugation, DMPE-PEG-maleimide was mixed with (non-reactive) DSPE-PEG at a 1:1 molar ratio and dissolved in an aqueous buffer to form micelles. Upon addition of nanobodies, stable non-reducible thioether bonds between nanobodies and the micelles are formed, increasing the molecular weight of the nanobodies as shown by Western blotting (Fig. 2A). Unmodified nanobodies typically displayed a single band at their molecular weight of 15–16 kD, which changed to a ladder-like pattern after conjugation to PEG-phospholipids. This pattern may be explained by the conjugation of one, two or multiple PEG-phospholipids (3.4 kD per unit) to each nanobody which alters their SDS-PAGE migration rate, and corresponds to previous reports in which nanobodies were attached to PEGylated liposomes [28,30]. Band intensities suggested that most nanobodies were conjugated to one or two PEG-phospholipid chains, and this modification pattern was similar for R2 and EGa1 nanobodies. The attachment of DMPE-PEG-maleimide to these nanobodies is not expected to compromise the interactions of the nanobodies with EGFR [28,30]. We then studied whether these micelles could be used to decorate the surface of EVs with nanobodies via post-insertion. Post-insertion of PEG-lipids into liposomes has been shown to be a temperature-dependent process, in which the efficiency of lipid incorporation improves with increasing temperature [34–37]. To test whether this mechanism would also apply to EVs, EVs derived from Neuro2A cells were mixed with nanobody-PEG micelles and incubated for 2 h at temperatures ranging from 4 °C to 60 °C. After incubation, EVs were purified from free micelles by size-exclusion chromatography (SEC) performed at 4 °C. Nanobody incorporation was assessed by Western blotting (Fig. 2B). When nanobody-PEG micelles in the absence of EVs were loaded onto the SEC column and typical EV fractions were analyzed, no nanobodies could be detected, indicating that the SEC method was suitable for complete separation of EVs from micelles (first lane in Fig. 2B). When untreated EVs were applied to the column, the same fractions showed the presence of commonly used EV marker proteins ALIX, TSG101 and CD9 [1] (second lane in Fig. 2B). Simple mixing of EVs with EGa1 nanobody resulted in a faint nanobody band in the EV sample, possibly due to co-elution of small nanobody aggregates.

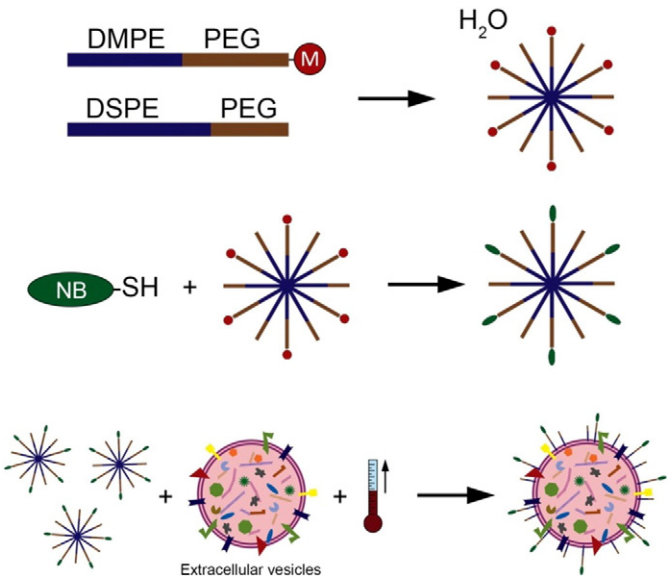

Fig. 1. Schematic representation of the protocol by which isolated extracellular vesicles are decorated with nanobodies via PEG-micellar post-insertion. Firstly, micelles are formed by dissolving phospholipid (DMPE and DSPE)-PEG derivatives in an aqueous buffer. DMPE-PEG is functionalized with a maleimide group (M). Secondly, nanobodies (NB) which are modified with sulfhydryl groups (-SH) are conjugated to the micelles via stable thioether bonds. Thirdly, nanobody-PEG micelles are mixed with isolated EVs and incubated at elevated temperatures (i.e. 40 °C), resulting in incorporation of nanobody-PEG-lipid into the vesicles. Picture is not drawn to scale.

However, when EVs were incubated with EGa1-PEG micelles, nanobody incorporation was dramatically increased. The efficiency of nanobody incorporation improved with increasing temperature, indicative of a post-insertion mechanism. In addition, incorporation of nanobodies conjugated to multiple lipid-PEG chains seemed to be increased at higher temperatures. Incubation at 60 °C, a common temperature for efficient post-insertion of PEG-lipids into liposomes [36,38], resulted in the highest association of nanobodies with EVs. However, as could be expected at this temperature, EV proteins showed signs of aggregation (illustrated by the appearance of a double ALIX band in Fig. 2B), and EV integrity and morphology were severely compromised as observed by electron microscopy (data not shown). Therefore, post-insertion at 40 °C was found to be optimal for nanobody incorporation while preserving EV characteristics. To further evaluate the degree of nanobody incorporation at this temperature, EVs modified with R2-PEG or EGa1-PEG micelles (EV-PEG-R2 and EV-PEG-EGa1, respectively) were analyzed by transmission electron microscopy (TEM) after immunogold labeling of the Myc-tags on the nanobodies (Fig. 2C). Unmodified EVs showed a typical cup-shaped morphology as seen in negative stain EM and were negative for immunogold labeling, while clear labeling of the EV surface was observed after post-insertion. Based on TEM images it was estimated that using these labeling conditions at least 7–14% of EVs contained one or more nanobodies, with both R2 and EGa1 nanobodies being incorporated at similar efficiencies. Furthermore, based on analysis of immuno-TEM images and Western blot band intensities, it was estimated that PEGylated EVs contained on average 0.4–4 nanobodies per EV. This theoretically corresponds with approximately 50–500 DMPE-PEG molecules per EV, assuming that micellar nanobody-conjugated DMPE-PEG inserted at similar efficiency into EVs as unconjugated DMPE-PEG. In addition, morphology and electron density of EVs after post-insertion were similar to untreated EVs, suggesting that insertion of PEG-lipids in EVs did not compromise EV integrity (Fig. 2D). This observation was supported by NTA data showing that EV size distribution was unaltered after post-insertion (Fig. 2E).

We hypothesized that the principle of post-insertion could also be applicable to EVs from other sources. To test this, EVs were isolated from platelets from healthy donors and subjected to post-insertion with EGa1-PEG micelles at different temperatures. A similar temperature-dependent nanobody-PEG-lipid incorporation was observed for platelet EVs (with optimal incorporation at 40 °C), while EV integrity was maintained (Supplementary Fig. 1). These data illustrate that EVs with distinct characteristics (e.g. origin, size, morphology) can be decorated with nanobody-conjugated PEG-lipids using the post-insertion method.

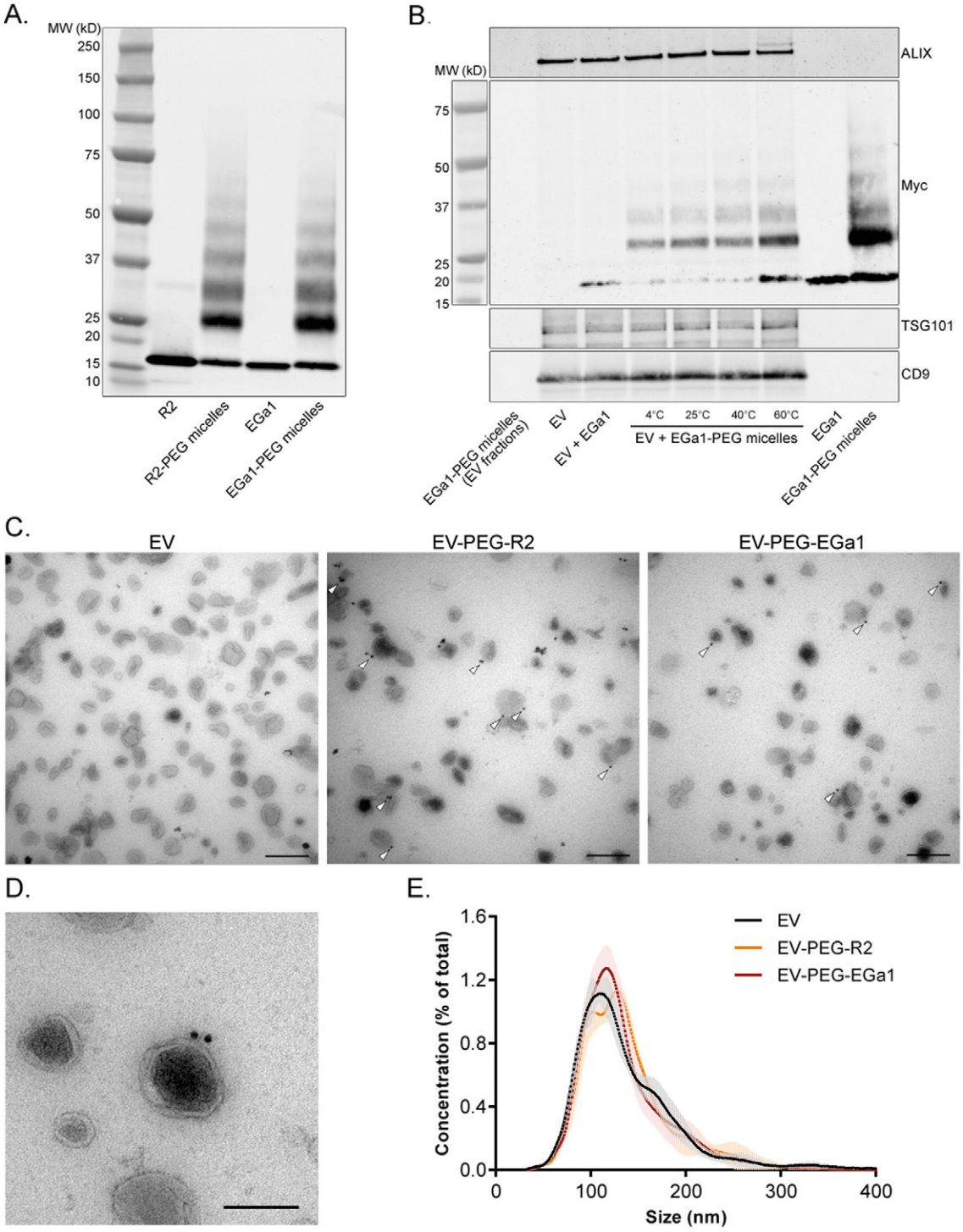

Fig. 2. EVs can be decorated with nanobodies using PEG-micellar post-insertion in a temperature dependent manner without loss of EV characteristics. A. Western blot analysis of Myc-tagged R2 and EGa1 nanobodies after coupling to DMPE-PEG-maleimide: DSPE-PEG (1:1) micelles. B. Western blot analysis of EV markers and nanobodies on Neuro2A EVs after post-insertion of EGa1-PEG micelles at various temperatures, and after purification with size-exclusion chromatography (SEC). Controls include concentrates of EV-fractions after SEC purification of EGa1-PEG micelles (first lane), untreated EVs (second lane), and EVs after incubation with EGa1 at 40 °C (third lane). EGa1 and EGa1-PEG micelles were loaded as a reference. C. Transmission electron microscopy images of EVs before and after post-insertion with R2-PEG and EGa1-PEG micelles. Grids were immunogold labeled with anti-Myc antibodies (arrowheads indicate membrane-associated gold). Scale bars represent 200 nm. D. High-magnification transmission electron microscopy image of EVs after post-insertion with EGa1-PEG micelles. Scale bar represents 100 nm. E. Size distribution of EVs before and after post-insertion, as analyzed by Nanoparticle Tracking Analysis. Data is shown as mean ± SD of 5 replicate measurements.

3.2. In vitro cell association of EVs after post-insertion with nanobody-PEG-lipids

To study whether post-insertion of nanobody-PEG-lipids affects EV-target cell interactions, Neuro2A-derived fluorescently labeled EVs were post-inserted with R2-PEG or EGa1-PEG micelles at various temperatures and incubated with A431 and Neuro2A cells. A431 cells overexpress EGFR, while Neuro2A cells lack EGFR expression (Fig. 3A). When post-insertion temperature was increased (improving nanobody-PEG-lipid incorporation), association of EVs with Neuro2A cells decreased, regardless of the nanobody used (Fig. 3B). When post-insertion was performed at 60 °C, cell binding was severely compromised, which

is in line with previous observations showing loss of EV integrity after post-insertion at this temperature. In contrast, binding of EVs to A431 cells was significantly increased after post-insertion with EGa1-PEG micelles, while insertion with R2-PEG micelles slightly decreased cell association when compared with unmodified EVs. The increase in cell binding after post-insertion with EGa1-PEG micelles correlated with EGa1 incorporation efficiency at different post-insertion temperatures. In this assay, it was confirmed that insertion at 40 °C was most efficient for optimal binding to A431 cells and this condition was therefore used in further experiments. Importantly, when EVs were incubated with EGa1 at 40 °C in the absence of lipid-PEG anchors, A431 cell binding was unaltered compared with unmodified controls. These data demonstrate that conjugation to lipid-PEG micelles is crucial for proper and functional anchoring of nanobodies to the surface of EVs.

3.3. In vivo circulation times and biodistribution of EVs after post-insertion with nanobody-PEG-lipids

Tissue distribution and related therapeutic efficacy of nanoparticles are largely determined by their circulation time [39]. PEGylation has been extensively applied to different types of nanoparticles in order to decrease deposition of plasma proteins on the particle surface, evade uptake by the RES and increase circulation time to boost their delivery potency [40,41]. We hypothesized that the introduction of PEG chains via post-insertion in EVs could have a similar effect on the circulation time of these particles. Multiple studies have shown that the circulation time of intravenously administered EVs is short compared with PEGylated liposomes (which can display circulation half-lives of up to several days [20]), with the majority of EVs being cleared within 60 min post-injection [22,42–45].

Neuro2A EVs were labeled with the lipophilic near-infrared dye DiR, purified, and subjected to post-insertion with R2-PEG and EGa1-PEG micelles. After removal of non-inserted DiR and micelles, 2.5 μg of EVs were intravenously administered to A431 tumor-bearing immunocompromised mice, and plasma samples were obtained at fixed time points after injection. It should be noted that the number of injected particles was comparable among EV samples, given that protein concentrations correlated well with particle concentrations as analyzed by NTA, regardless of the presence of PEG and nanobodies (2.5 μg of protein corresponded to approximately $2 * 10^{10}$ particles). To evaluate EV circulation time, DiR fluorescence signals in plasma were compared with a calibration curve of known concentrations of the injected batch of DiR-labeled EVs spiked in blank plasma. As expected, unmodified EVs were rapidly removed from blood plasma, and were below detection threshold 10 min post-injection (Fig. 4A). In contrast, when EVs were PEGylated via post-insertion with R2-PEG or EGa1-PEG micelles, circulation time was significantly increased. Modified EVs were still detectable in plasma of all mice 60 min post-injection, and some mice even showed plasma DiR signal at 240 min post-injection. These kinetics were similar when a higher dose (i.e. 6 μg of EVs) was administered (Supplementary Fig. 2). Such an increase in circulation time could have important implications for tumor accumulation. Organs of tumor-bearing mice intravenously injected with DiR-labeled EV were harvested and analyzed 4 h post-injection (Fig. 4B). EVs showed a typical nanoparticle-like biodistribution pattern, with the vast majority of the signal partitioning to the major RES organs liver and spleen. For other organs (kidneys, lungs, brain and tumor), DiR signals from EVs were below the detection limit. When organs were analyzed 1 h post-injection, a similar pattern was observed (data not shown). This is in correspondence with previous reports on EV biodistribution [22,46]. After post-insertion of the EVs with nanobody-PEG micelles, organ distribution was unaltered compared with unmodified EVs. A small increase in spleen compared with liver accumulation was observed, which may be due to increased exposure of the PEGylated EVs to circulating monocytes and macrophages [47].

4. Discussion

In this study we show that nanobodies can be introduced onto EVs from two distinct sources (Neuro2A tumor cells and platelets) using a PEG-micellar post-insertion strategy. While EVs maintained their morphologic and biophysical characteristics, the insertion of nanobody-coupled PEG chains had important implications for in vitro and in vivo interactions of EVs with their environment. We found that EV–cell interactions in vitro were strongly reduced by PEG, but could be specifically recovered or even enhanced for EGFR-expressing cells when EGFR-binding nanobodies (EGa1) were attached to the distal end of PEG chains. This effect has also been described for synthetic PEGylated particles in previous studies [48,49]. These data suggest that EVs were specifically redirected to EGFR-expressing tumor cells, while evading interactions with other cells. Given that EVs are reported to be readily taken up by a variety of cell types, and targeting specificity appears to be only subtle or unpredictable [10,50,51], combined PEGylation and targeting could be a valuable advancement towards the use of EVs as cell- or tissue-specific drug carriers. Evasion of uptake by non-targeted cells could minimize the occurrence of off-target effects

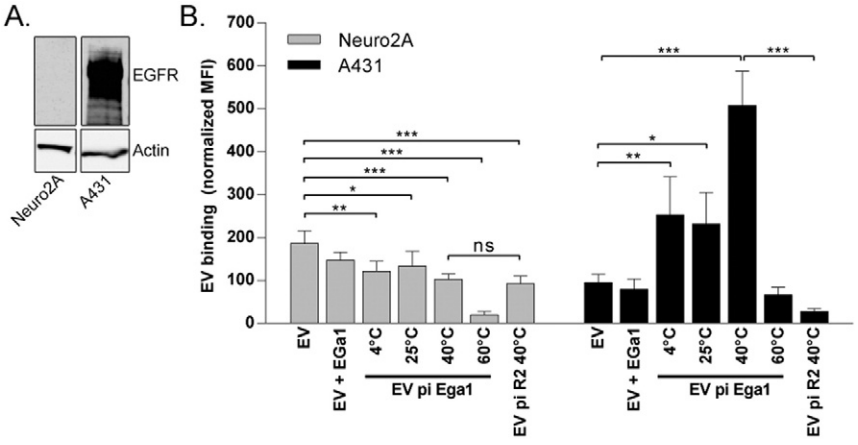

Fig. 3. Post-insertion of EVs with R2-PEG micelles decreases EV binding to Neuro2A and A431 cells, while post-insertion with EGa1-PEG micelles specifically increases binding to EGFR-overexpressing A431 cells. A. Western blot analysis of EGFR expression in Neuro2A and A431 cells. Actin is shown as a loading control. B. Binding of CellTracker Deep Red-labeled Neuro2A EVs to Neuro2A and A431 cells, after post-insertion (pi) with R2-PEG or EGa1-PEG micelles at various temperatures, determined by flow cytometry. A control in which EVs were incubated with unconjugated EGa1 at 40 °C and purified by size-exclusion chromatography was included (EV + Ega1). Representative data of at least three replicate experiments are shown, and data are displayed as mean ± SD. ns = not significant, * represents $p < 0.05$, ** $p < 0.01$, and *** $p < 0.001$ using one-way ANOVA with Tukey post-hoc test.

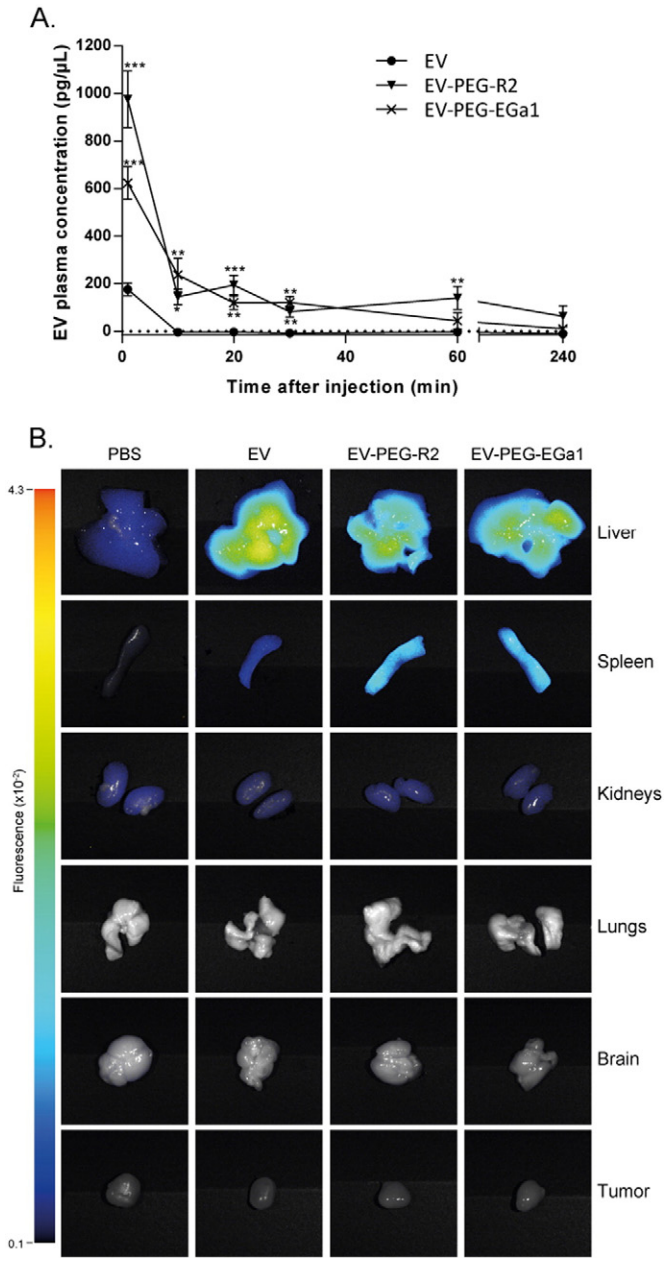

Fig. 4. Post-insertion with nanobody-PEG micelles increases EV circulation time and does not affect general biodistribution. A. Plasma concentration of DiR-labeled Neuro2A EVs before and after post-insertion with nanobody-PEG micelles, measured at several time points after i.v. injection of 2.5 μg of EVs in tail veins of Crl:NU-Foxn1^{nu} mice. Dotted line indicates lower detection threshold. B. Representative fluorescence/white field overlay Pearl Impulse images of organs from mice injected i.v. with 6 μg of DiR-labeled Neuro2A EVs, harvested 4 h post-injection. Results in A are expressed as mean ± SEM, n = 3–6. * represents $p < 0.05$, ** $p < 0.01$, and *** $p < 0.001$ compared with EV group at the same time point using one-way ANOVA with Tukey post-hoc test.

and promote therapeutic efficacy. However, PEGylation has been described to impede the escape of nanoparticles from endosomal compartments after internalization, resulting in lysosomal degradation instead of functional delivery of the cargo (e.g. therapeutic nucleic acids) [52–54]. Furthermore, PEGylated EVs, targeted with EGa1 nanobodies, would be expected to be taken up via EGFR-dependent endocytosis [30], while their natural counterparts may be taken up via other routes (e.g. lipid-raft mediated endocytosis or macropinocytosis [10]). On the other hand, the present study shows that the post-insertion procedure is relatively mild, and does not noticeably affect EV integrity or protein composition. It is therefore conceivable that the potency of EVs to functionally deliver their cargo is retained to some extent after PEGylation. This is an important advantage of EVs compared with their synthetic counterparts (i.e. liposomes), which are often characterized by poor intracellular delivery efficiency, which further declines upon PEGylation [39,55,56]. Whether PEGylated and retargeted EVs can still promote functional cargo delivery through their unique composition remains to be elucidated and may be a subject for further studies.

The RES has been shown to be responsible for the clearance of the majority of nanoparticulate systems [20,57,58], and has also been implicated in the clearance of exogenously administered EVs [42]. We show that PEGylation of EVs results in a significant increase in circulation time in mice, suggesting that PEGylated EVs avoided plasma protein opsonization and phagocytosis by cells from the RES. We expected that this would result in an increased passive accumulation of these EVs in tumor tissue due to extravasation through leaky tumor vasculature (commonly known as the enhanced-permeability-and-retention (EPR) effect [20,39,59]). After successful migration into the tumor tissue, the presence of EGFR-specific nanobodies was hypothesized to promote retention of the EVs in the tumor tissue and facilitate entry into tumor cells. Unfortunately, EV PEGylation did not result in a detectable increase in tumor accumulation. This may be explained by technical detection limitations in this study. Stringent EV purification protocols in our study limited the EV dose that could be administered to $2–5 * 10^{10}$ particles/mouse, which is approximately 10-fold lower than reported in similar studies [46]. This, together with the fact that we assessed tumor accumulation at an earlier time point (4 h versus 24 h after injection [46]), may have prevented any accumulated EV signal from reaching the detection threshold. The use of a reporter system with higher sensitivity than DiR, such as the recently described *Gaussia* luciferase-based reporter [22], may aid to better evaluate the effect of EV PEGylation on tumor accumulation.

It was roughly estimated that PEGylated EVs contained on average 50–500 PEG-DMPE molecules per EV. This is similar to the calculated amount of exterior-facing PEG chains in 100 nm unilamellar liposomes formulated with 0.5–1 mol% of PEG-lipids, assuming that these liposomes contain on average 80,000 lipids per vesicle. Despite this substantial PEG grafting density, which has been shown to confer shielding properties to liposomes [60,61], EV plasma concentrations still steeply declined by >80% within 10 min after injection. This could correspond with the observation that after post-insertion only a minority of all EVs contained nanobodies (and therefore PEG) as estimated using TEM. It could also be that only subtypes of EVs with a specific protein/lipid composition are amenable to post-insertion, that post-inserted lipids gradually partitioned out of the EV membranes, or that the insertion protocol needs further optimization. In this study, DMPE-PEG(3400) phospholipids were employed. The advantage of phospholipids with such short acyl chains (14 carbon atoms) is their ability to readily transfer to lipid bilayer membranes at temperatures compatible with biological systems [62]. This is crucial in order to maintain EV integrity, given that EV integrity was severely compromised upon incubation at elevated temperatures (60 °C). Unfortunately, post-inserted short-chain phospholipids have also been described to readily partition out of liposomes, especially in the presence of serum proteins [62,63]. This may have resulted in a gradual loss of 'stealth' properties in vivo and consequently affected circulation half-life. The plasma stability of post-inserted DMPE-PEG in EV membranes was not investigated in the current study, however it is conceivable that the stability of exogenously introduced lipids is different in EV membranes compared with liposomes due to their unique membrane composition [39]. EVs are typically enriched in membrane-stabilizing lipids, such as cholesterol, sphingomyelin and ganglioside GM3 [2,64], which may improve retention of inserted PEG-lipids [63,65]. To possibly increase PEG stability in the EV membrane, PEGylated phospholipids with longer acyl chains (e.g. 16 or 18 carbon atoms, DPPE or DSPE, respectively) could be used for post-insertion. These have been described to show improved

anchoring properties compared with DMPE when employed in liposomes, however at the cost of post-insertion efficiency at physiological temperatures [62,63,66]. These mechanisms are also likely to apply to EVs, given that in preliminary experiments post-insertion with DSPE-PEG was less efficient than post-insertion with DMPE-PEG (data not shown). Hence, a trade-off between PEG grafting density and anchor stability may exist. Furthermore, the efficiency of post-insertion is also determined by the length of the PEG chains, with shorter PEG chains being inserted in liposomes with higher efficiency than longer PEG chains [66], while longer PEG chains have been described to better shield particles from clearance by the RES [20]. In addition, optimization of the number of PEG chains and targeting ligands per particle may be crucial to balance proper cell entry with sufficient shielding properties [67,68]. These parameters could be considered as starting points to further improve the stable and functional insertion of PEGylated targeting ligands in EVs.

Given that the described post-insertion strategy may be used to target EVs to specific cell types while avoiding interactions with others and also increasing circulation time, our data highlight possibilities for future research. PEGylated EVs could be employed to increase accumulation at sites of inflammation in other pathologies, such as rheumatoid arthritis and inflammatory bowel diseases, which are characterized by localized increased vascular permeability [69]. In addition, the ease of ligand coupling to functionalized PEG-phospholipids allows for application of a range of targeting ligands (e.g. well-studied RGD peptides to target angiogenic endothelial cells [70] or clinically approved antibodies against established tumor targets [71]). Taken together, decoration of EVs with PEG-coupled targeting ligands via post-insertion is a promising new tool to improve the potential of EVs for drug delivery.

Acknowledgments

The work of SAAK, LALF, PV and RMS on cell-derived membrane vesicles is supported by a European Research Council starting grant (260627) “MINDS” in the FP7 ideas program of the European Union. PV is supported by a VENI Fellowship (# 13667) from The Netherlands Organisation for Scientific Research (NWO). RvdM is supported by a funding from the European Union's Horizon 2020 research and innovation program under the Marie Skłodowska-Curie grant agreement no 660426. C.W. Seinen is gratefully acknowledged for the technical assistance in electron microscopy experiments.

Appendix A. Supplementary data

Supplementary data to this article can be found online at http://dx.doi.org/10.1016/j.jconrel.2016.01.009.

References

[1] S. El-Andaloussi, I. Mager, X.O. Breakefield, M.J. Wood, Extracellular vesicles: biology and emerging therapeutic opportunities, Nat. Rev. Drug Discov. 12 (2013) 347–357.
[2] S.A. Kooijmans, P. Vader, S.M. van Dommelen, W.W. van Solinge, R.M. Schiffelers, Exosome mimetics: a novel class of drug delivery systems, Int. J. Nanomedicine 7 (2012) 1525–1541.
[3] S.M. van Dommelen, P. Vader, S. Lakhal, S.A. Kooijmans, W.W. van Solinge, M.J. Wood, R.M. Schiffelers, Microvesicles and exosomes: opportunities for cell-derived membrane vesicles in drug delivery, J. Control. Release 161 (2012) 635–644.
[4] P. Vader, X.O. Breakefield, M.J. Wood, Extracellular vesicles: emerging targets for cancer therapy, Trends Mol. Med. 20 (2014) 385–393.
[5] C. Thery, M. Ostrowski, E. Segura, Membrane vesicles as conveyors of immune responses, Nat. Rev. Immunol. 9 (2009) 581–593.
[6] H.F. Heijnen, A.E. Schiel, R. Fijnheer, H.J. Geuze, J.J. Sixma, Activated platelets release two types of membrane vesicles: microvesicles by surface shedding and exosomes derived from exocytosis of multivesicular bodies and alpha-granules, Blood 94 (1999) 3791–3799.
[7] K. Denzer, M.J. Kleijmeer, H.F. Heijnen, W. Stoorvogel, H.J. Geuze, Exosome: from internal vesicle of the multivesicular body to intercellular signaling device, J. Cell Sci. 113 (Pt 19) (2000) 3365–3374.
[8] B. Gyorgy, M.E. Hung, X.O. Breakefield, J.N. Leonard, Therapeutic applications of extracellular vesicles: clinical promise and open questions, Annu. Rev. Pharmacol. Toxicol. 55 (2015) 439–464.
[9] J.G. van den Boorn, M. Schlee, C. Coch, G. Hartmann, SiRNA delivery with exosome nanoparticles, Nat. Biotechnol. 29 (2011) 325–326.
[10] L.A. Mulcahy, R.C. Pink, D.R. Carter, Routes and mechanisms of extracellular vesicle uptake, J Extracell Vesicles, 3, 2014.
[11] L. Alvarez-Erviti, Y. Seow, H. Yin, C. Betts, S. Lakhal, M.J. Wood, Delivery of siRNA to the mouse brain by systemic injection of targeted exosomes, Nat. Biotechnol. 29 (2011) 341–345.
[12] J. Wahlgren, L.K.T. De, M. Brisslert, F. Vaziri Sani, E. Telemo, P. Sunnerhagen, H. Valadi, Plasma exosomes can deliver exogenous short interfering RNA to monocytes and lymphocytes, Nucleic Acids Res. 40 (2012), e130.
[13] S. Ohno, M. Takanashi, K. Sudo, S. Ueda, A. Ishikawa, N. Matsuyama, K. Fujita, T. Mizutani, T. Ohgi, T. Ochiya, N. Gotoh, M. Kuroda, Systemically injected exosomes targeted to EGFR deliver antitumor microRNA to breast cancer cells, Mol. Ther. 21 (2013) 185–191.
[14] V. Gujrati, S. Kim, S.H. Kim, J.J. Min, H.E. Choy, S.C. Kim, S. Jon, Bioengineered bacterial outer membrane vesicles as cell-specific drug-delivery vehicles for cancer therapy, ACS Nano 8 (2014) 1525–1537.
[15] K. Tang, Y. Zhang, H. Zhang, P. Xu, J. Liu, J. Ma, M. Lv, D. Li, F. Katirai, G.X. Shen, G. Zhang, Z.H. Feng, D. Ye, B. Huang, Delivery of chemotherapeutic drugs in tumour cell-derived microparticles, Nat. Commun. 3 (2012) 1282.
[16] S.C. Jang, O.Y. Kim, C.M. Yoon, D.S. Choi, T.Y. Roh, J. Park, J. Nilsson, J. Lotvall, Y.K. Kim, Y.S. Gho, Bioinspired exosome-mimetic nanovesicles for targeted delivery of chemotherapeutics to malignant tumors, ACS Nano 7 (2013) 7698–7710.
[17] M.E. Hung, J.N. Leonard, Stabilization of exosome-targeting peptides via engineered glycosylation, J. Biol. Chem. 290 (2015) 8166–8172.
[18] Y. Tian, S. Li, J. Song, T. Ji, M. Zhu, G.J. Anderson, J. Wei, G. Nie, A doxorubicin delivery platform using engineered natural membrane vesicle exosomes for targeted tumor therapy, Biomaterials 35 (2014) 2383–2390.
[19] T.M. Allen, P. Sapra, E. Moase, Use of the post-insertion method for the formation of ligand-coupled liposomes, Cell. Mol. Biol. Lett. 7 (2002) 889–894.
[20] J.S. Suk, Q. Xu, N. Kim, J. Hanes, L.M. Ensign, PEGylation as a strategy for improving nanoparticle-based drug and gene delivery, Adv. Drug Deliv. Rev. (2015).
[21] J.V. Jokerst, T. Lobovkina, R.N. Zare, S.S. Gambhir, Nanoparticle PEGylation for imaging and therapy, Nanomedicine (London, England) 6 (2011) 715–728.
[22] C.P. Lai, O. Mardini, M. Ericsson, S. Prabhakar, C.A. Maguire, J.W. Chen, B.A. Tannous, X.O. Breakefield, Dynamic biodistribution of extracellular vesicles in vivo using a multimodal imaging reporter, ACS Nano 8 (2014) 483–494.
[23] F. Ciardiello, G. Tortora, EGFR antagonists in cancer treatment, N. Engl. J. Med. 358 (2008) 1160–1174.
[24] N. Tebbutt, M.W. Pedersen, T.G. Johns, Targeting the ERBB family in cancer: couples therapy, Nat. Rev. Cancer 13 (2013) 663–673.
[25] H. Revets, P. De Baetselier, S. Muyldermans, Nanobodies as novel agents for cancer therapy, Expert. Opin. Biol. Ther. 5 (2005) 111–124.
[26] S. Ewert, C. Cambillau, K. Conrath, A. Pluckthun, Biophysical properties of camelid V(HH) domains compared to those of human V(H)3 domains, Biochemistry 41 (2002) 3628–3636.
[27] E. Dolk, C. van Vliet, J.M. Perez, G. Vriend, H. Darbon, G. Ferrat, C. Cambillau, L.G. Frenken, T. Verrips, Induced refolding of a temperature denatured llama heavy-chain antibody fragment by its antigen, Proteins 59 (2005) 555–564.
[28] R. van der Meel, S. Oliveira, I. Altintas, R. Haselberg, J. van der Veeken, R.C. Roovers, P.M. van Bergen en Henegouwen, G. Storm, W.E. Hennink, R.M. Schiffelers, R.J. Kok, Tumor-targeted Nanobullets: Anti-EGFR nanobody-liposomes loaded with anti-IGF-1R kinase inhibitor for cancer treatment, J. Control. Release 159 (2012) 281–289.
[29] F.W. Studier, Protein production by auto-induction in high density shaking cultures, Protein Expr. Purif. 41 (2005) 207–234.
[30] S. Oliveira, R.M. Schiffelers, J. van der Veeken, R. van der Meel, R. Vongpromek, P.M. van Bergen en Henegouwen, G. Storm, R.C. Roovers, Downregulation of EGFR by a novel multivalent nanobody-liposome platform, J. Control. Release 145 (2010) 165–175.
[31] S.A. Kooijmans, S. Stremersch, K. Braeckmans, S.C. de Smedt, A. Hendrix, M.J. Wood, R.M. Schiffelers, K. Raemdonck, P. Vader, Electroporation-induced siRNA precipitation obscures the efficiency of siRNA loading into extracellular vesicles, J. Control. Release 172 (2013) 229–238.
[32] E.G. Hofman, M.O. Ruonala, A.N. Bader, D. van den Heuvel, J. Voortman, R.C. Roovers, A.J. Verkleij, H.C. Gerritsen, P.M. van Bergen en Henegouwen, EGF induces coalescence of different lipid rafts, J. Cell Sci. 121 (2008) 2519–2528.
[33] S. Oliveira, G.A. van Dongen, M. Stigter-van Walsum, R.C. Roovers, J.C. Stam, W. Mali, P.J. van Diest, P.M. van Bergen en Henegouwen, Rapid visualization of human tumor xenografts through optical imaging with a near-infrared fluorescent anti-epidermal growth factor receptor nanobody, Mol. Imaging 11 (2012) 33–46.
[34] T. Perrier, P. Saulnier, F. Fouchet, N. Lautram, J.P. Benoit, Post-insertion into Lipid NanoCapsules (LNCs): from experimental aspects to mechanisms, Int. J. Pharm. 396 (2010) 204–209.
[35] P.S. Uster, T.M. Allen, B.E. Daniel, C.J. Mendez, M.S. Newman, G.Z. Zhu, Insertion of poly(ethylene glycol) derivatized phospholipid into pre-formed liposomes results in prolonged in vivo circulation time, FEBS Lett. 386 (1996) 243–246.
[36] T. Ishida, D.L. Iden, T.M. Allen, A combinatorial approach to producing sterically stabilized (Stealth) immunoliposomal drugs, FEBS Lett. 460 (1999) 129–133.
[37] K. Nakamura, K. Yamashita, Y. Itoh, K. Yoshino, S. Nozawa, H. Kasukawa, Comparative studies of polyethylene glycol-modified liposomes prepared using different PEG-modification methods, Biochim. Biophys. Acta 1818 (2012) 2801–2807.
[38] J.N. Moreira, T. Ishida, R. Gaspar, T.M. Allen, Use of the post-insertion technique to insert peptide ligands into pre-formed stealth liposomes with retention of binding activity and cytotoxicity, Pharm. Res. 19 (2002) 265–269.
[39] R. van der Meel, M.H. Fens, P. Vader, W.W. van Solinge, O. Eniola-Adefeso, R.M. Schiffelers, Extracellular vesicles as drug delivery systems: lessons from the liposome field, J. Control. Release 195 (2014) 72–85.

[40] A. Puri, K. Loomis, B. Smith, J.H. Lee, A. Yavlovich, E. Heldman, R. Blumenthal, Lipid-based nanoparticles as pharmaceutical drug carriers: from concepts to clinic, Crit. Rev. Ther. Drug Carrier Syst. 26 (2009) 523–580.
[41] L. Zhang, F.X. Gu, J.M. Chan, A.Z. Wang, R.S. Langer, O.C. Farokhzad, Nanoparticles in medicine: therapeutic applications and developments, Clin. Pharmacol. Ther. 83 (2008) 761–769.
[42] T. Imai, Y. Takahashi, M. Nishikawa, K. Kato, M. Morishita, T. Yamashita, A. Matsumoto, C. Charoenviriyakul, Y. Takakura, Macrophage-dependent clearance of systemically administered B16BL6-derived exosomes from the blood circulation in mice, J. Extracell. Vesicles 4 (2015) 26238.
[43] S.C. Saunderson, A.C. Dunn, P.R. Crocker, A.D. McLellan, CD169 mediates the capture of exosomes in spleen and lymph node, Blood 123 (2014) 208–216.
[44] M. Morishita, Y. Takahashi, M. Nishikawa, K. Sano, K. Kato, T. Yamashita, T. Imai, H. Saji, Y. Takakura, Quantitative analysis of tissue distribution of the B16BL6-derived exosomes using a streptavidin–lactadherin fusion protein and iodine-125-labeled biotin derivative after intravenous injection in mice, J. Pharm. Sci. 104 (2015) 705–713.
[45] Y. Takahashi, M. Nishikawa, H. Shinotsuka, Y. Matsui, S. Ohara, T. Imai, Y. Takakura, Visualization and in vivo tracking of the exosomes of murine melanoma B16-BL6 cells in mice after intravenous injection, J. Biotechnol. 165 (2013) 77–84.
[46] O.P. Wiklander, J.Z. Nordin, A. O'Loughlin, Y. Gustafsson, G. Corso, I. Mager, P. Vader, Y. Lee, H. Sork, Y. Seow, N. Heldring, L. Alvarez-Erviti, C.E. Smith, K. Le Blanc, P. Macchiarini, P. Jungebluth, M.J. Wood, S.E. Andaloussi, Extracellular vesicle in vivo biodistribution is determined by cell source, route of administration and targeting, J. Extracell. Vesicles 4 (2015) 26316.
[47] S.W. Jones, R.A. Roberts, G.R. Robbins, J.L. Perry, M.P. Kai, K. Chen, T. Bo, M.E. Napier, J.P. Ting, J.M. Desimone, J.E. Bear, Nanoparticle clearance is governed by Th1/Th2 immunity and strain background, J. Clin. Invest. 123 (2013) 3061–3073.
[48] P. Vader, B.J. Crielaard, S.M. van Dommelen, R. van der Meel, G. Storm, R.M. Schiffelers, Targeted delivery of small interfering RNA to angiogenic endothelial cells with liposome-polycation-DNA particles, J. Control. Release 160 (2012) 211–216.
[49] S.D. Li, L. Huang, Targeted delivery of antisense oligodeoxynucleotide and small interference RNA into lung cancer cells, Mol. Pharm. 3 (2006) 579–588.
[50] D. Zech, S. Rana, M.W. Buchler, M. Zoller, Tumor-exosomes and leukocyte activation: an ambivalent crosstalk, Cell Commun. Signal. : CCS 10 (2012) 37.
[51] K.J. Svensson, H.C. Christianson, A. Wittrup, E. Bourseau-Guilmain, E. Lindqvist, L.M. Svensson, M. Morgelin, M. Belting, Exosome uptake depends on ERK1/2-heat shock protein 27 signaling and lipid Raft-mediated endocytosis negatively regulated by caveolin-1, J. Biol. Chem. 288 (2013) 17713–17724.
[52] K. Remaut, B. Lucas, K. Braeckmans, J. Demeester, S.C. De Smedt, Pegylation of liposomes favours the endosomal degradation of the delivered phosphodiester oligonucleotides, J. Control. Release 117 (2007) 256–266.
[53] R.N. Majzoub, C.L. Chan, K.K. Ewert, B.F. Silva, K.S. Liang, E.L. Jacovetty, B. Carragher, C.S. Potter, C.R. Safinya, Uptake and transfection efficiency of PEGylated cationic liposome-DNA complexes with and without RGD-tagging, Biomaterials 35 (2014) 4996–5005.
[54] N.N. Sanders, L. Peeters, I. Lentacker, J. Demeester, S.C. De Smedt, Wanted and unwanted properties of surface PEGylated nucleic acid nanoparticles in ocular gene transfer, J. Control. Release 122 (2007) 226–235.
[55] H. Hillaireau, P. Couvreur, Nanocarriers' entry into the cell: relevance to drug delivery, Cell. Mol. Life Sci. 66 (2009) 2873–2896.
[56] T.M. Allen, P.R. Cullis, Liposomal drug delivery systems: from concept to clinical applications, Adv. Drug Deliv. Rev. 65 (2013) 36–48.
[57] D.E. Owens 3rd, N.A. Peppas, Opsonization, biodistribution, and pharmacokinetics of polymeric nanoparticles, Int. J. Pharm. 307 (2006) 93–102.
[58] R. van der Meel, L.J. Vehmeijer, R.J. Kok, G. Storm, E.V. van Gaal, Ligand-targeted particulate nanomedicines undergoing clinical evaluation: current status, Adv. Drug Deliv. Rev. 65 (2013) 1284–1298.
[59] S.D. Li, L. Huang, Nanoparticles evading the reticuloendothelial system: role of the supported bilayer, Biochim. Biophys. Acta 1788 (2009) 2259–2266.
[60] R.M. Schiffelers, I.A. Bakker-Woudenberg, G. Storm, Localization of sterically stabilized liposomes in experimental rat *Klebsiella pneumoniae* pneumonia: dependence on circulation kinetics and presence of poly(ethylene)glycol coating, Biochim. Biophys. Acta 1468 (2000) 253–261.
[61] N. Dos Santos, C. Allen, A.M. Doppen, M. Anantha, K.A. Cox, R.C. Gallagher, G. Karlsson, K. Edwards, G. Kenner, L. Samuels, M.S. Webb, M.B. Bally, Influence of poly(ethylene glycol) grafting density and polymer length on liposomes: relating plasma circulation lifetimes to protein binding, Biochim. Biophys. Acta 1768 (2007) 1367–1377.
[62] W.M. Li, L. Xue, L.D. Mayer, M.B. Bally, Intermembrane transfer of polyethylene glycol-modified phosphatidylethanolamine as a means to reveal surface-associated binding ligands on liposomes, Biochim. Biophys. Acta 1513 (2001) 193–206.
[63] G.N. Chiu, M.B. Bally, L.D. Mayer, Effects of phosphatidylserine on membrane incorporation and surface protection properties of exchangeable poly(ethylene glycol)-conjugated lipids, Biochim. Biophys. Acta 1560 (2002) 37–50.
[64] Y.J. Yoon, O.Y. Kim, Y.S. Gho, Extracellular vesicles as emerging intercellular communicasomes, BMB Rep. 47 (2014) 531–539.
[65] N. Golkar, A.M. Tamaddon, S.M. Samani, Effect of lipid composition on incorporation of trastuzumab-PEG-lipid into nanoliposomes by post-insertion method: physicochemical and cellular characterization, J. Liposome Res. (2015) 1–13.
[66] K. Shimada, S. Matsuo, Y. Sadzuka, A. Miyagishima, Y. Nozawa, S. Hirota, T. Sonobe, Determination of incorporated amounts of poly(ethylene glycol)-derivatized lipids in liposomes for the physicochemical characterization of stealth liposomes, Int. J. Pharm. 203 (2000) 255–263.
[67] J.M. Saul, A. Annapragada, J.V. Natarajan, R.V. Bellamkonda, Controlled targeting of liposomal doxorubicin via the folate receptor in vitro, J. Control. Release 92 (2003) 49–67.
[68] M. Rabenhold, F. Steiniger, A. Fahr, R.E. Kontermann, R. Ruger, Bispecific single-chain diabody-immunoliposomes targeting endoglin (CD105) and fibroblast activation protein (FAP) simultaneously, J. Control. Release 201 (2015) 56–67.
[69] H. Nehoff, N.N. Parayath, L. Domanovitch, S. Taurin, K. Greish, Nanomedicine for drug targeting: strategies beyond the enhanced permeability and retention effect, Int. J. Nanomedicine 9 (2014) 2539–2555.
[70] K. Temming, R.M. Schiffelers, G. Molema, R.J. Kok, RGD-based strategies for selective delivery of therapeutics and imaging agents to the tumour vasculature, Drug Resist. Updat. 8 (2005) 381–402.
[71] P.M. Glassman, J.P. Balthasar, Mechanistic considerations for the use of monoclonal antibodies for cancer therapy, Cancer Biol. Med. 11 (2014) 20–33.